(3) the leading edges (high $\bar{\nu}$ values). From experience, this procedure resulted in fits that were not as well fit at low energies as at higher energies. However, in the low-energy region anharmonicity effects and errors arising from truncation of the sums in eq A5 are enhanced and as a consequence the deviations at low energies do not appear to affect in a serious way the values of the parameters derived from the spectral fits.

Attempts at nonlinear least-squares fitting of the spectra using published procedures[40] were generally unsuccessful. Problems appear to arise because the parameters are not entirely independent in that variations in one parameter may necessitate rather large changes in the others and because it is difficult to devise an algorithm that allows a computer to decide on quality of fit based, for example, on the criteria described above. The procedure that we have followed has been to examine the calculated spectrum after each iteration and, on the basis of how well it fits, choose the parameters for the next iteration. The procedure was repeated until a "good fit" (as defined above) was obtained. Standard deviations for each parameter were calculated by using the "good-fit" parameters in a nonlinear least-squares program, constrained to 0 iterations (immediate convergence). The validity of the approach lies in the consistency of the results. It should be noted that by now the approach described here has been used by a number of people who without previous knowledge of the "correct" parameters have all arrived at essentially the same values. As an illustration, in Figure 6 are shown the "good" fits for $Os(bpy)_3^{2+}$, the least-squares-generated fit, and fits obtained by varying S_M, $\bar{\nu}_M$, S_L, and $\bar{\nu}_{1/2}$ by ±10%. Clearly, Figure 6A is the best fit and it provided the parameters used in the text.

(40) Johnson, K. J. "Numerical Methods in Chemistry"; Marcel Dekker: New York, 1980.

Registry No. $Os(bpy)_3^{2+}$, 23648-06-8; $Os(bpy)_2(P_2)^{2+}$, 75441-74-6; $Os(bpy)(P_2)_2^{2+}$, 89711-31-9; $Ru(bpy)_3^{2+}$, 15158-62-0; $Ru(bpy)_2(en)^{2+}$, 47597-15-9; *fac*-Re(bpy)(CO)$_3$Cl, 55658-96-3.

Synthesis, Proton NMR Spectroscopy, and Structural Characterization of Binuclear Ruthenium Porphyrin Dimers

James P. Collman,*† Craig E. Barnes,† Paul N. Swepston,‡ and James A. Ibers*‡

Contribution from the Departments of Chemistry, Stanford University, Stanford, California 94305, and Northwestern University, Evanston, Illinois 60201.
Received August 4, 1983

Abstract: The binuclear Ru(II) porphyrin dimers $(Ru(OEP))_2$ and $(Ru(TPP))_2$ (OEP = 2,3,7,8,12,13,17,18-octaethylporphyrinato; TPP = 5,10,15,20-tetraphenylporphyrinato) have been synthesized by the vacuum pyrolysis of the mononuclear bis(pyridine) complexes $Ru(OEP)(py)_2$ and $Ru(TPP)(py)_2$ (py = pyridine). A detailed analysis of the paramagnetic shifts observed in the ^1H NMR spectra is presented, and a new model for referencing dipolar shifts in a dimeric porphyrin structure type is described. The calculated contact shifts exhibit π symmetry and indicate that the dominant mode of spin transfer into the porphyrin ring is derived from P $3e(\pi) \rightarrow$ Ru charge transfer. In addition, the crystal structure of the OEP dimer is reported. $(Ru(OEP))_2$ crystallizes as the dipentane solvate in space group C_{2h}^6-$C2/c$ with $Z = 8$ in a unit cell of dimensions $a = 27.989$ (11) Å, $b = 27.255$ (12) Å, $c = 17.737$ (8) Å, and $\beta = 102.50$ (2)°. The final agreement indices, based on 767 variables and 9806 unique intensities collected at −103 °C on an automatic diffractometer, are $R(F^2) = 0.066$ and $R_w(F^2) = 0.124$. The conventional R index on F for 7304 reflections having $F^2 > 3\sigma(F_o^2)$ is 0.042. The distance between the Ru atoms is 2.408 (1) Å and the mean Ru-N distance is 2.050 (5) Å. Each Ru atom is situated 0.30 Å out of a plane defined by four coordinating N atoms in the direction of the other Ru atom. The two porphyrin macrocycles are twisted 23.8 (1)° with respect to each other. Both porphyrinato cores have domed-type distortions with average deviations from the least-squares planes of 0.07 and 0.10 Å and maximum deviations of 0.19 and 0.24 Å, respectively. The X-ray and NMR results are consistent with a qualitative MO diagram that suggests a formal Ru-Ru bond order of 2.

Investigations into the chemistry of ruthenium porphyrins have, until now, been narrowly focused. This is surprising in view of the interesting and highly diversified chemistry that iron porphyrins are known to exhibit.[1] One factor in explaining this difference is the lack of easily prepared ruthenium(II) porphyrin complexes that do not contain the coordinatively inert carbonyl ligand. The carbonyl ligand is known to back-bond so strongly to ruthenium porphyrins that it exerts an overwhelming influence on the chemistry of these complexes.[2] Thus it is of great interest to develop new synthetic entries into ruthenium porphyrin chemistry that either bypass the carbonyl adduct or effectively utilize it to form complexes having more interesting ligands.

Two methods of removing the carbonyl ligand have been reported. Hopf et al.[3] were first to describe the photochemical ejection of CO from ruthenium porphyrins to produce a ruthenium(II) bis(pyridine) complex. Although this reaction proceeds in good yield, it is difficult to exchange cleanly the bound pyridine groups for more weakly binding ligands. In addition, a photolysis of this type is limited to those ligands that can withstand prolonged exposure to intense UV irradiation.

Recently, we[4] and others[5] described an oxidative method for removing the carbonyl ligand. The reaction of a ruthenium(II) porphyrin, Ru(P)(CO)L,[6] with *tert*-butyl hydroperoxide gives an

†Stanford University.
‡Northwestern University.

(1) Scheidt, W.; Reed, C. *Chem. Rev.* **1981**, *81*, 543-555.
(2) Brown, G.; Hopf, F.; Meyer, T.; Whitten, D. *J. Am. Chem. Soc.* **1975**, *97*, 5385-5390.
(3) Hopf, F. R.; O'Brien, T.; Scheidt, W.; Whitten, D. *J. Am. Chem. Soc.* **1975**, *97*, 277-281.
(4) Collman, J. P.; Barnes, C. E; Collins, T. J.; Brothers, P. J.; Gallucci, J.; Ibers, J. A. *J. Am. Chem. Soc.* **1981**, *103*, 7030-7032.
(5) Masuda, H.; Taga, T.; Osaki, K.; Sugimoto, H.; Mori, M.; Ogoshi, H. *J. Am. Chem. Soc.* **1981**, *103*, 2199-2202.
(6) Abbreviations used: P = porphyrinato dianion in general; OEP = 2,3,7,8,12,13,17,18-octaethylporphyrinato; TPP = 5,10,15,20-tetraphenylporphyrinato; TTP = 5,10,15,20-tetra-*p*-tolylporphyrinato; T-*n*-PrP = 5,10,15,20-tetra-*n*-propylporphyrinato; H_{meso} = meso protons of OEP; H_β = β-pyrrolic protons of a TPP type porphyrin; H_o, $H_{o'}$, H_m, $H_{m'}$, H_p, $H_{p\text{-}CH_3}$ = ortho, ortho′, meta, meta′, para, para-methyl substituents on a meso phenyl ring for which the "top" and "bottom" of the phenyl rings are chemically distinct; py = pyridine; MO = molecular orbital; AO = atomic orbital; L = axial ligand in general; Me_4Si = tetramethylsilane.

0002-7863/84/1506-3500$01.50/0

air-stable oxo-bridged ruthenium(IV) porphyrin dimer in good yield. We have found that this dimer is reduced by a variety of chemical reductants to afford a divalent ruthenium porphyrin complex that contains labile axial ligands. We are currently investigating the scope of these reactions and will report our results in the near future.

In another segment of our investigations into the properties of ruthenium porphyrins we have discovered and characterized an interesting ruthenium(II) porphyrin dimer containing a multiple metal–metal bond.[4] The crucial step in the preparation of these ruthenium porphyrin dimers is the solid-state pyrolysis of ruthenium(II) bis(pyridine) porphyrin precursors in which the *analytically pure* product is obtained in nearly *quantitative* yield. These highly air-sensitive[4] ruthenium dimers readily bind a wide variety of ligands in the absence of oxygen, quantitatively producing the corresponding monomeric ruthenium(II) bis(L) porphyrins.

Herein we report details of the synthesis of $(Ru(OEP))_2$ and $(Ru(TPP))_2$ and an analysis of the paramagnetic shifts observed in their proton NMR spectra. In addition, the X-ray crystallographic study of $(Ru(OEP))_2$ is described. A preliminary account of the synthetic and spectral work has appeared.[4]

Experimental Section

Reagents and Solvents. All solvents were of reagent grade and were used without further purification. NMR solvents were stored in flasks sealed with Teflon stopcocks with vacuum adaptors. Benzene-d_6 and toluene-d_8 were stored in the presence of benzophenone ketyl.

Proton NMR Spectra. Proton NMR spectra for the compounds reported herein were recorded on three instruments: (1) a 100-MHz Varian XL-100 modified to operate as a pulse instrument with the use of a Nicolet Technology Corp. Model 1180 FT disk data system; (2) a 300-MHz wide-bore Nicolet Supercon with a Model 1280e FT disk data system; (3) a modified 360-MHz Bruker spectrometer with an Oxford Magnetics Supercon magnet and a Nicolet 1180 disk data system.

Samples of air-sensitive compounds for NMR analysis were prepared either in a Vacuum Atmospheres inert-atmosphere box where the continuously measured level of oxygen was <2 ppm or on a high-vacuum line (10^{-5} torr) where deuterated solvents were vapor transferred into an NMR tube that was then sealed under vacuum.

The preparation and characterization of ruthenium(II) carbonyl porphyrins have been described.[7,8] The general method we have developed for inserting ruthenium into the porphyrins reported on here is a modification of the procedure of Chow and Cohen[7] and is described for $H_2(OEP)$.

Carbonyl(methanol)(octaethylporphyrinato)ruthenium(II) (1). $H_2(OEP)$ (1 g, 1.8 mmol) is dissolved in 500 mL of boiling ethyl digol, 2-(2-methoxyethoxy)ethanol, under a carbon monoxide atmosphere. $RuCl_3 \cdot H_2O$ (940 mg, 2 equiv) was dissolved in 50 mL of ethyl digol and added dropwise to the boiling solution over 3 h. The final solution was heated at reflux for an additional 2 h. The extent of reaction was measured by TLC (SiO_2:CH_2Cl_2) or UV/vis spectra of aliquots of the reaction mixture. Note: a competing side reaction to insertion is reduction of ruthenium to Ru(0), which is observed as a mirror on the sides of the flask. When no free-base porphyrin could be detected by TLC or UV/vis spectroscopy, the solution was cooled and flushed with argon. The volume was reduced to 50 mL on a rotary evaporator, at which time 100 mL of distilled water was quickly added to precipitate all porphyrinic material. The solution was filtered through Celite, and the residue was washed with water, dried, and redissolved in CH_2Cl_2. Silica gel, 100 cm^3, was added to the vigorously stirred solution. Filtering away the silica gel yielded a translucent bright red solution for which TLC showed one pink spot (R_f 0.98) with no origin material. The solution volume was reduced to 200 mL, at which time 40 mL of methanol plus 10 drops of water were added. The solution volume was further reduced to 50 mL and refrigerated overnight. The crystals that formed were filtered, washed with methanol, and dried under vacuum. The product, isolated as carbonyl(methanol)(octaethylporphyrinato)ruthenium(II), exhibited properties identical with those reported by Hopf et al.[3] Yield on a 1-g scale: 780 mg (60%). Anal. Calcd for $C_{38}H_{48}N_4O_2Ru$: C, 65.77; H, 6.97; N, 8.07. Found: C, 65.53; H, 7.02; N, 8.31. NMR ($CDCl_3$, 100 MHz): H_{meso} 9.95 (s), CH_2 4.11 (7.6 Hz q), CH_3 1.94 (7.6 Hz q), OCH_3 −2.3 (s), $HOCH_3$ −0.5 (bs) ppm. IR (KBr): 1945, 1928 cm^{-1} (CO). UV/vis (C_6H_6) (λ_{max}, nm (log ϵ)): 393 (5.16) (Soret), 517 (4.06), 549 (4.38).

Carbonyl(methanol)(tetraphenylporphyrinato)ruthenium(II) (2).[8] Yield on a 500-mg scale: 438 mg (70%). NMR ($CDCl_3$, 100 MHz): H_β 8.67 (s), H_o 8.18 (m), H_m 7.71 (m), H_p 7.71 (m), OCH_3 −4 (s), $HOCH_3$ ~0.0 (bs) ppm. UV/vis (λ_{max}, nm): 412 (Soret), 532. IR (KBr): 1930 cm^{-1} (CO).

The preparation and characterization of ruthenium(II) bis(pyridine) porphyrins have been reported by Hopf et al.,[3] Antipas et al.,[9] and Chow and Cohen.[7] We followed the method of Antipas et al. to prepare the complexes described below.

Bis(pyridine)(octaethylporphyrinato)ruthenium(II) (3). Yield on a 100-mg scale: 105 mg (95%). Anal. Calcd for $C_{45}H_{54}N_6Ru$: C, 69.66; H, 6.87; N, 10.61. Found: C, 69.19; H, 6.86; N, 10.45. NMR (C_6D_6, 360 MHz): H_{meso} 9.69 (s), CH_2 3.92 (7.6 Hz q), CH_3 1.96 (7.6 Hz q), pyridine: H_o 2.23 (7.2 Hz d), H_m 4.11 (7.2 Hz t), H_p 4.64 (7.2 Hz t) ppm. MS: $(M - py)^+$ *m/e* 713, $(M - 2py)^+$ 634. UV/vis (C_6H_6) (λ_{max}, nm): 394 (Soret), 386 (sh), 406 (sh), 452, 494, 521.

Bis(pyridine)(tetraphenylporphyrinato)ruthenium(II) (4). Yield based on 100-mg scale: 100 mg (90%). NMR (C_6D_6, 100 MHz): H_β 8.61 (s), H_o 8.2 (m), H_m 7.48 (m), H_p 7.48 (m), pyridine: H_o 2.92 (7.3 Hz d), H_m 4.48 (7.4 Hz t), H_p 5.19 (7.3 Hz t) ppm. UV/vis (C_6H_6) (λ_{max}, nm): 412 (Soret), 422, 505.

Bis((octaethylporphyrinato)ruthenium(II)) (5). Solid $Ru(OEP)(py)_2$ 100 mg, 0.126 mmol) was heated to 210 °C under high vacuum (10^{-5} torr) overnight. The solid changed from brick red to dull green. The loose, air-sensitive solid product was separated from sublimed material on the sides of the flask. The product prepared in this way was analytically pure. Yield: 76 mg (95%). Anal. Calcd for $C_{72}H_{88}N_8Ru_2$: C, 68.10; H, 6.99; N, 8.84. Found: C, 67.90; H, 7.00; N, 8.75. NMR (C_6D_6, 100 MHz, 30 °C): H_{meso} 10.14 (s), CH_2 25.51 (m), 11.0 (m), CH_3 3.42 (7.5 Hz t) ppm. UV/vis (C_6H_6, λ_{max}, nm (log ϵ)): 373 (4.95) (Soret), 503 (3.9), 527 (3.89), 545 (sh), 650 (3.66), 624 (3.72).

Bis((tetraphenylporphyrinato)ruthenium(II)) (6). The crystalline bis(pyridine) adduct obtained from the photolysis reaction[7] must be transformed into an amorphous state before the pyrolysis reaction is attempted. A convenient method to accomplish this was a lyophilization procedure wherein the crystalline solid (100 mg) was first dissolved in a benzene–pyridine (99:1) solution (heating may be required). This solution was quickly frozen with a liquid nitrogen cooling bath. The resulting ice and the sample were allowed to warm to room temperature under vacuum. The benzene and pyridine slowly sublimed, leaving the amorphous bis(pyridine) solid. This solid was pyrolyzed as described for $(Ru(OEP))_2$. The product, $(Ru(TPP))_2$, was obtained analytically pure in 95% yield (78 mg). Anal. Calcd for $C_{88}H_{56}N_8Ru_2$: C, 74.04; H, 3.95; N, 7.85. Found: C, 74.49; H, 3.90; N, 7.63. NMR (toluene-d_8, 360 MHz, 22 °C): H_β −14.21 (s), H_o +6.59 (7 Hz d), H_m +7.63 (7 Hz t), H_p +8.71 (7 Hz t), $H_{m'}$ +9.41 (7 Hz t), $H_{o'}$ +13.35 (7 Hz d) ppm. UV/vis (C_6D_6) (λ_{max}, nm): 385 (Soret) 522, 730.

Bis((tetra-*p*-tolylporphyrinato)ruthenium(II)). This complex was prepared in the manner of the TPP analogue (6). NMR (C_6D_6, 25 °C): H_β −14 (s), H_o 7.2 (7 Hz d), H_m 7.3 (7 Hz d), *p*-CH_3 2.45 (s), $H_{m'}$ 7.8 (7 Hz d), $H_{o'}$ 9.7 (7 Hz d) ppm.

X-ray Analysis of $(Ru(OEP))_2 \cdot 2C_5H_{12}$ (5). Crystals of the Ru dimer suitable for X-ray work were obtained through recrystallization from a pentane solution. After a preliminary photographic examination (precession and Weissenberg) we concluded that the crystals belong to a centered monoclinic space group (C_s^4-*Cc* or C_{2h}^6-*C*2/*c*). Reflections of the type *hkl* with *h* odd and *k* odd are systematically weak but observable. Accurate unit cell parameters were determined by least-squares refinement of 16 reflections (22.9° <2θ(Mo Kα) < 32.8°) that had been automatically centered on a Picker FACS-I diffractometer. Data collection was performed in a standard manner.[10] Crystallographic and experimental details are given in Table I.

The selection of the proper temperature for data collection was crucial to this experiment. By cooling the crystal slowly from room temperature we found that the material undergoes a reversible transition at approximately −140 °C. Above this temperature the peaks are sharp and have good intensity; below it the peaks broaden considerably. To be safe a temperature of ~−100 (actually −103 °C) was selected for data collection.

The centrosymmetric space group *C*2/*c* was assumed to be the correct space group after an evaluation of the statistical distribution of the normalized structure factors. When separated into parity classes the average values of $|E|^2$ were indicative of a sublattice arrangement of Ru atoms; the average values of $|E|^2$ for the odd–odd–even and odd–odd–odd

(7) Chow, B.; Cohen, I. *Bioinorg. Chem.* **1971**, *1*, 57.
(8) Bonnet, J. J.; Eaton, S. S.; Eaton, G. R.; Holm, R. H.; Ibers, J. A. *J. Am. Chem. Soc.* **1973**, *95*, 2141–2149.
(9) Antipas, A.; Buchler, J. W.; Gouterman, M.; Smith, P. D. *J. Am. Chem. Soc.* **1978**, *100*, 3015–3024.
(10) See, for example: Waters, J. M.; Ibers, J. A. *Inorg. Chem.* **1977**, *16*, 3273–3277.

Table I. Crystallographic Data

formula	$C_{72}H_{88}Ru_2N_8 \cdot 2C_5H_{12}$
formula wt, amu	1412.00
space group	C_{2h}^6-$C2/c$
a, Å	27.99 (1)
b, Å	27.25 (1)
c, Å	17.737 (8)
β, deg	102.50 (2)
vol, Å^3	13 209
Z	8
temp[a]	−103 °C
radiation	Mo Kα (λ(Kα_1) = 0.7093 Å, graphite monochromator)
linear abs coeff, cm^{-1}	4.92
transmission factors[b]	0.839–0.928
bounding planes	{010}, {021}, {001}, (100), ($\bar{3}$10)
crystal vol, mm^3	0.0426
detector aperture	3.5 mm wide × 5.0 mm high; 32 cm from crystal
takeoff angle, deg	3.3
scan speed	2°/min in 2θ
scan range	0.7° below Kα_1 to 1.2° above Kα_2
2θ limits, deg	$3.7 \leq 2\theta \leq 47.0$
bkgd counts	10 s at each end of scan with rescan option[c]
data collected	$\pm h, -k, +l$
unique data (including $F_o^2 < 0$)	9134
unique data with $F_o^2 > 3\sigma(F_o^2)$	7304
final no. of variables	767
$R(F^2)$	0.065
$R_w(F^2)$	0.122
error in observation of unit weight, e^2	1.783
R (on F for $F_o^2 > 3\sigma(F_o^2)$)	0.042

[a] The low-temperature system is based on a design by Huffman, J. C. Ph.D. Thesis, Indiana University, 1974. [b] The numbers given are the distances in millimeters between the Friedel pairs. [c] The diffractometer was run under the Vanderbilt disk-oriented system (Lenhert, P. G. *J. Appl. Crystallogr.* 1975, *8*, 568–570).

parity classes were only 10% as large as the average values for the even-even-odd and even-even-even parity classes. In our hands the structure proved to be an extremely difficult one to solve. Owing to the subcell of Ru atoms ab initio direct-methods programs failed. The problem is well-known: the weak parity classes arise from small deviations of the Ru positions from the symmetry of the subcell and from deviations of the entire molecule from a higher symmetry, and these two effects are difficult to separate although solution of the structure requires that this separation be made. Once we recognized the problem we turned to Patterson methods. Interpretation of the origin-removed sharpened Patterson map led to eight possible solutions for the Ru atom positions. Four of these solutions involved two independent half-molecules in the asymmetric unit while the other four solutions involved one independent dimer in the asymmetric unit. For all eight solutions the Ru atoms contributed only to the even-even-even and even-even-odd reflections and provided no phasing information about the other parity classes. Refinement of the two Ru and eight N positions derived from these eight solutions provided minimal clues as to which was the correct solution. It was therefore necessary to develop the entire model; we accomplished this by means of the direct-methods program DIRDIF.[11] Refinement of each of these complete or nearly complete structural models revealed one that gave a sensible geometry and acceptable residuals. When the correct Ru atom positions were used, all 80 of the N and C atoms belonging to the dimer were located after one cycle of DIRDIF.

Conventional atomic scattering factors were used for the non-hydrogen[12] and hydrogen[13] atoms. Anomalous dispersion corrections[14] were applied to the Ru atoms with values of $\Delta f'$ and $\Delta f''$ of Cromer and Waber.[12] An analytical absorption correction was applied to the intensities as was an overall linear decay correction of 1%.

The model refined isotropically to an R value of 9.7%. At this point two independent disordered pentane molecules were detected in a difference electron density map. The C_γ atom of each pentane molecule is situated on a crystallographic 2-fold axis, with the two independent solvent molecules being separated by (0, $^1/_2$, 0). Each solvent molecule is disordered about the $C_\alpha \cdots C_\gamma \cdots C_\alpha$ axis and thus only the C_α and C_γ atoms are resolved. The solvent molecules were modeled by including discrete anisotropic C_α and C_γ atoms and fixed contributions to the structure factors for freely rotating C_β atoms. After anisotropic refinement of the porphyrin dimer model, hydrogen atoms were located in difference electron density maps. Idealized hydrogen positions (C–H = 0.95 Å; H–C–H = 109.5°) were either calculated (non-methyl) or obtained from a least-squares adjustment of the observed position (methyl) and were added as fixed contributions to the structure factors. Each hydrogen atom was assigned an isotropic thermal parameter 1 Å^2 greater than the equivalent isotropic thermal parameter of the atom to which it is attached. Solvent hydrogen atoms were not included in this model.

The final cycle of full-matrix least-squares refinement involved 767 variables and 9134 unique intensities. The function minimized was $\sum(F_o^2 - k^2F_c^2)^2/\sigma^2(F_o^2)$, where F_o and F_c are the observed and calculated structure factors and where k is the scale factor. The final residuals are $R(F_o^2) = 0.065$ and $R_w(F_o^2) = 0.122$, and error in an observation of unit weight is 1.78 e^2. The conventional R indices on F_o for the 7304 reflections having $F_o^2 > 3\sigma(F_o^2)$ are $R(F_o) = 0.042$ and $R_w(F_o) = 0.064$. All calculations were performed on a Harris 800 computer with programs standard at Northwestern University.

The positional parameters for the non-hydrogen atoms are listed in Table II.[15] The anisotropic thermal parameters (Table III), the hydrogen atom positions (Table IV), and the final values of $10|F_o|$ and $10|F_c|$ (Table V) are available as supplementary material.[15] A negative entry in Table V implies that F_o^2 was observed to be negative.

Results

Synthesis. Ruthenium may be inserted into porphyrin free bases via the ruthenium(II) chlorocarbonyl dimer $[RuCl_2(CO)_3]_2$, which is generated in situ by slowly adding a solution of ruthenium trichloride in ethyl digol (2-(2-methoxyethoxy)ethanol) to a boiling solution of the free base in the same solvent under CO. The resulting ruthenium(II) porphyrin is isolated as the carbonyl complex. By the method of Antipas et al.,[9] irradiation of the carbonyl complex in pyridine yields the bis(pyridine) ruthenium(II) porphyrin in good yield.

$$[RuCl_2(CO)_3]_2 + H_2P \xrightarrow{\Delta} RuP(CO)(MeOH)$$
1, P = OEP
2, P = TPP

$$RuP(CO)(MeOH) + py \xrightarrow{h\nu} RuP(py)_2$$
3, P = OEP
4, P = TPP

When the bis(pyridine) complexes **3** and **4**[16] are heated under high vacuum pyridine is lost and the title compounds, $(Ru(OEP))_2$ and $(Ru(TPP))_2$, are formed.

$$RuP(py)_2 \xrightarrow[\text{vacuum}]{\Delta} (Ru(P))_2$$
5, P = OEP
6, P = TPP

Proton NMR Spectra. The proton NMR spectra of $(Ru(OEP))_2$ (**5**) and $(Ru(TPP))_2$ (**6**) have been described previously.[4] Table VI summarizes the observed isotropic shifts for **5** and **6**. The overall appearance of the spectra of **5** and **6** indicates that these complexes possess effective 4-fold symmetry and that the porphyrin macrocycle has not been degraded under the conditions of the vacuum pyrolysis. The individual resonances could be assigned through the observation of well-resolved spin–spin splittings and decoupling experiments. The α-methylene proton resonances of the OEP macrocycle are observed as two identical, coupled multiplets shifted far downfield from their normal, dia-

(11) DIRDIF: *Dir*ect methods applied to *Dif*ference structure factors to strengthen Fourier methods. Beurskens, P. T.; Bosman, W. P.; Doesburg, H. M.; Gould, R. O.; van den Hark, Th. E. M.; Prick, P. A. J. "Computational Crystallography"; Sayre, D., Ed.; Clarendon Press: Oxford, **1982**; p 516.
(12) Cromer, D. T.; Waber, J. T. "International Tables for X-ray Crystallography"; Kynoch Press: Birmingham, England, 1974; Vol. IV p 71.
(13) Stewart, R. F.; Davidson, E. R.; Simpson, W. T. *J. Chem. Phys.* **1965**, *42*, 3175–3187.
(14) Ibers, J. A.; Hamilton, W. C. *Acta Crystallogr.* **1964**, *17*, 781–782.
(15) See supplementary material paragraph at end of paper.
(16) See footnote 13 in ref. 4.

Table VI. Observed Isotropic Shifts for Ruthenium Porphyrin Dimers $(Ru(P))_2$[a]

			meso-aryl							
P	H_β	H_{meso}	H_o	H_m	H_p	$H_{m'}$	$H_{o'}$	*p*-CH_3	αCH_2	αCH_3
TPP	−23		−0.8	0.4	1.1	1.2	3.7			
TTP	−22.8		−0.7	0.3		1.5	3.6	1.0		
OEP		0.9							21.3 7.0	1.5

[a] The observed isotropic shift is defined here by $\Delta\delta_{iso}{}^{obsd} = \Delta\delta_{obsd}{}^{para} - \Delta\delta_{obsd}{}^{dia}$, where $\Delta\delta_{obsd}{}^{para}$ is the observed shift for a particular proton in the paramagnetic case and $\Delta\delta_{obsd}{}^{dia}$ is the corresponding shift for a suitable diamagnetic reference compound. We have obtained the diamagnetic shifts used here from the analogous rhodium(II) porphyrin dimers.[17] $\Delta\delta_o{}^{dia} = 7.2$; $\Delta\delta_m{}^{dia} = 7.3$; $\Delta\delta_p{}^{dia} \sim 7.6$; $\Delta\delta_{m'}{}^{dia} = 7.8$; $\Delta\delta_{o'}{}^{dia} = 9.7$; $\Delta\delta_{p\text{-}CH_3}{}^{dia} = 2.45$; $\Delta\delta_\beta{}^{dia} = 8.7$. OEP: $\Delta\delta_{\alpha CH_2}{}^{dia} = 4.5, 4.0$; $\Delta\delta_{\alpha CH_3}{}^{dia} = 1.75$; $\Delta\delta_{meso}{}^{dia} = 9.2$. Sample conditions: benzene-d_6 or toluene-d_8, 25 °C.

magnetic positions[17] and separated from one another by *more than* 10 ppm at room temperature. The diastereotropic nature of these protons indicates that mirror symmetry in the plane of the porphyrin has been lost. This is true in the solid-state structure of $(Ru(OEP))_2$, as will be discussed below. Evidence for the loss of this plane of symmetry is also found in the spectrum of the TPP analogue (**6**). Slow rotation[18] of the meso phenyl rings and loss of mirror symmetry in the porphyrin plane cause the phenyl proton resonances to be observed as a set of five well-resolved doublets and triplets, each exhibiting a 7-Hz ortho spin–spin splitting. Partial assignment of each phenyl resonance is based on the multiplicity of each signal because of spin–spin splitting, decoupling experiments, and comparison with the *meso-p*-tolyl (TTP) analogue of **6**. As an example, assignment of the para phenyl proton is considered. From the schematic representation of **6**, the para

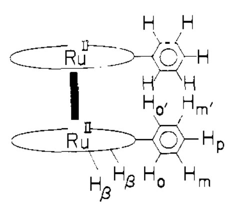

phenyl proton is expected to appear as a triplet because of equivalent coupling to both adjacent meta protons. Irradiation of the para proton resonance should cause both meta proton resonances to collapse into doublets owing to coupling with the adjacent ortho protons. Experimentally this behavior is observed when the triplet at +8.7 ppm (downfield from Me_4Si) is irradiated. Finally, comparison of the phenyl resonances with the TTP analogue in which the resonace at +8.7 ppm is not found verifies this assignment.

The above three criteria do not, however, lead to unambiguous assignments for each member of the ortho, ortho′ and meta, meta′ pairs of doublets and triplets. Additional information provided by our analysis of the paramagnetic dipolar shifts experienced by these positions (vide infra) differentiates the ortho and ortho′ resonances with respect to their relative orientations toward the two ruthenium atoms in these dimers. The assignments of these resonances listed in Table VI are based on this analysis.

The proton NMR resonance shifts for $(Ru(OEP))_2$ and $(Ru(TPP))_2$ were observed to be independent of solvent (toluene or benzene) and concentration at room temperature. The β-pyrrolic-H resonance for $(Ru(TPP))_2$ is observed ~14 ppm upfield of Me_4Si with a line width of 2.8 Hz at room temperature. The proton line widths observed for these dimers are the smallest yet reported for paramagnetic metalloporphyrin complexes. Assuming dominant dipolar relaxation,[19] we estimate the electron spin–lattice relaxation time T_{1e} to be less than 2×10^{-13} s. This short T_{1e} undoubtedly arises from zero-field-splitting modulation in solution

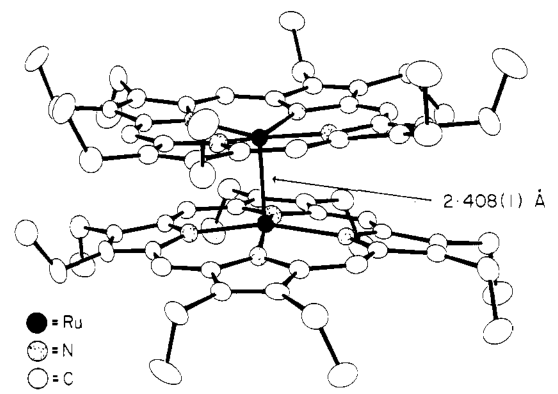

Figure 1. Drawing of $(Ru(OEP))_2$. The hydrogen atoms have been omitted for clarity and the vibrational ellipsoids are drawn at the 50% probability level.

for the ground-state triplet system.[19]

Crystal Structure of $(Ru(OEP))_2 \cdot 2C_5H_{12}$. The motivation underlying our study of this crystal structure arises from a general interest in the forces that govern the geometry of the porphyrin macrocycle. Structural characterization of $(Ru(OEP))_2$ provides us with information about a unique metal–metal bonded system and the way in which two metalloporphyrins distort when forced to make very close contact. There is considerable interest in both intramolecular[5,20,21] and intermolecular[22,23] porphyrin interactions.

The molecular structure of $(Ru(OEP))_2$ is illustrated in Figure 1 and can be described as two cofacial ruthenium octaethylporphyrin groups bound together by a ruthenium–ruthenium bond. The halves of the dimer differ from each other in terms of ethyl group orientations; for one porphyrin macrocycle two of the peripheral ethyl groups are oriented toward the center of the molecule while for the other porphyrin only one ethyl group is oriented in this manner. There is no evidence for side-chain disorder, as is known for octaethylporphyrins.[24] The crystal packing for $(Ru(OEP))_2 \cdot 2C_5H_{12}$ is displayed in Figure 2 (supplementary) material[15]); the molecules are well separated, with all contacts of the non-hydrogen atoms being greater than 3.44 Å.

Each porphyrin skeleton has a domed conformation, with displacement of the ruthenium atom from the plane of the four coordinating nitrogen atoms (0.30 Å for both Ru atoms) in the direction of the other ruthenium atom. Deviations from the 24-atom mean porphyrin planes along with the atom-numbering scheme are presented in Figure 3. The average (0.08 and 0.10 Å) and maximum (0.206 (4) and 0.245 (4) Å) displacements from the porphyrin plane are consistent with other metalloporphyrins that exhibit domed distortions.[25] The difference between the

(17) Collman, J. P.; Barnes, C. E.; Woo, L. K. *Proc. Natl. Acad. Sci. U.S.A.* **1983**, *80*, 7684–7688.
(18) Eaton, S. S.; Fishwild, D. M.; Eaton, G. R. *Inorg. Chem.* **1978**, *17*, 1542–1545.
(19) Swift, T. J. In "NMR of Paramagnetic Molecules"; La Mar, G. N., Horrocks, W. D., Jr., Holm, R. H., Eds.; Academic Press: New York, 1973; Chapter 2.

(20) Collman, J. P.; Elliott, C. M.; Halbert, T. R.; Tovrog, B. S. *Proc. Natl. Acad. Sci. U.S.A.* **1977**, *74*, 18–22.
(21) Kagan, N. E.; Mauzerall, D.; Merrifield, R. B. *J. Am. Chem. Soc.* **1977**, *99*, 5484–5486.
(22) Kutzler, F. W.; Swepston, P. N.; Berkovitch-Yellin, Z.; Ellis, D. E.; Ibers, J. A. *J. Am. Chem. Soc.* **1983**, *105*, 2996–3004.
(23) Masuda, H.; Taga, T.; Osaki, K.; Sugimoto, H.; Yoshida, Z.; Ogoshi, H. *Inorg. Chem.* **1980**, *19*, 950–955.
(24) Little, R. G.; Ibers, J. A. *J. Am. Chem. Soc.* **1974**, *96*, 4452–4463.

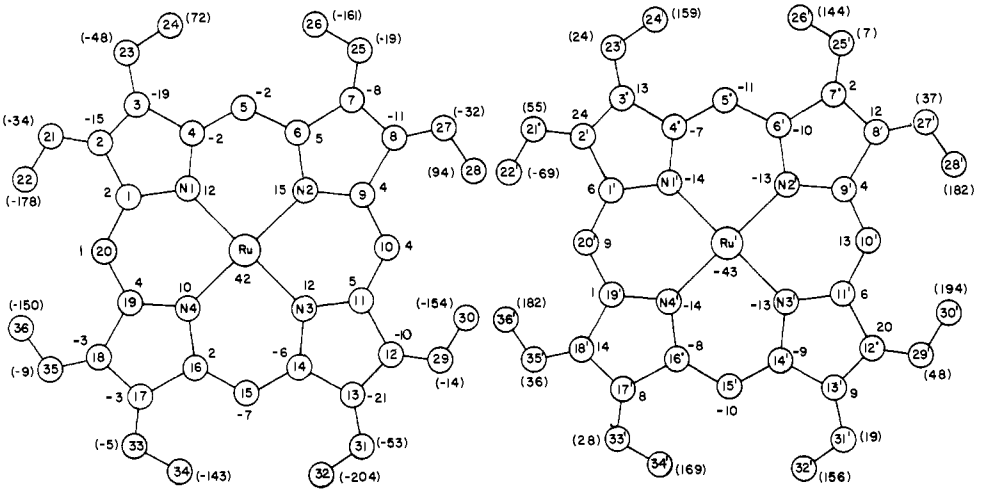

Figure 3. Displacements ($\times 10^3$ Å) of atoms from the weighted least-squares planes of the 24-atom porphyrin skeletons. The estimated standard deviations are 0.003 Å for nitrogen atoms and 0.004 Å for carbon atoms.

distance of the metal center from the least-squares plane of the 24-atom skeleton and from the plane of the four porphyrinato nitrogen atoms, often called the doming parameter,[26] is approximately equal (0.12 and 0.13 Å) for the halves of the dimer. This metal-to-plane separation is usually attributed to occupancy of the $d_{x^2-y^2}$ orbital for five-coordinate metalloporphyrin complexes. However, in this case the 0.30-Å out-of-plane displacement of each Ru atom more likely is caused by intramolecular porphyrin–porphyrin repulsion. (See discussion below.)

The two porphyrin skeletons are essentially parallel (dihedral angle between the two 24-atom cores is 0.2°) with an interplanar separation of 3.26 Å. The porphyrin cores are twisted by 23.8 (1)°.[27] In the structure of $[(OEP)Ru(OH)]_2O$[5] the halves of the dimer are twisted by 22.7° and are separated by 3.71 Å. Since the domed distortions of the porphyrin skeletons in $(Ru(OEP))_2$ are significant and the crystallographically unique porphyrinato core in $[(OEP)Ru(OH)]_2O$ is essentially planar, a comparison of interplanar atomic separations rather than distances between porphyrin best planes is desirable. It is not surprising that the shortest interplanar atomic distances[28] for $(Ru(OEP))_2$ involve nitrogen atoms (mean N···N′ = 3.119 (4) Å; range = 3.108 (4)–3.146 (4) Å). But surprisingly the C_a···C_m and C_a···N separations are similar (mean C_a···C_m = 3.28 (1) Å, range = 3.199 (6)–3.359 (6) Å; mean C_a···N = 3.26 (1) Å, range = 3.229 (5)–3.287 (5) Å). All of the other distances are significantly longer (mean C_a···C_b = 3.567 (4) Å; mean C_b···C_m = 3.555 (4) Å; mean C_b···C_b = 3.461 (4) Å) and in only one case does the shortest contact involve an ethyl β-carbon atom (C(8)···C(26)′ = 3.600 (7) Å). In contrast, in $[(OEP)Ru(OH)]_2O$ all contacts are longer, with the C_b···C_b (3.72 Å) and C_a···C_m (3.74 Å) distances being shorter than the N···N (3.84 Å) contacts.

The small interplanar separation observed for $(Ru(OEP))_2$ indicates that significant orbital overlap between the porphyrin aromatic systems is possible. The similar twist angles observed here and by Masuda et al.[5] for $[(OEP)Ru(OH)]_2O$ in the solid state support the hypothesis that specific π–π^* interactions between the highest occupied and lowest unoccupied MO's of the porphyrin macrocycles occur. Spectroscopically, the observed broadening and shift to the blue of the Soret band for $(Ru(OEP))_2$ are also indicative of significant excitonic interactions between the porphyrin macrocycles.[29]

Table VII. Selected Bond Distances (Å) for $(Ru(OEP))_2$

atoms	porphyrin 1	porphyrin 2	mean
Ru–Ru	2.408 (1)		
Ru–N(1)	2.054 (3)	2.052 (3)	Ru–N = 2.050 (5)
Ru–N(2)	2.057 (3)	2.051 (3)	
Ru–N(3)	2.043 (3)	2.045 (3)	
Ru–N(4)	2.049 (3)	2.046 (3)	
N(1)–C(1)	1.384 (5)	1.377 (5)	$N-C_a$ = 1.377 (7)
N(1)–C(4)	1.366 (5)	1.375 (5)	
N(2)–C(6)	1.376 (5)	1.366 (5)	
N(2)–C(9)	1.368 (5)	1.380 (5)	
N(3)–C(11)	1.388 (5)	1.378 (5)	
N(3)–C(14)	1.379 (5)	1.381 (5)	
N(4)–C(16)	1.380 (5)	1.375 (5)	
N(4)–C(19)	1.374 (5)	1.388 (5)	
C(1)–C(2)	1.453 (6)	1.436 (6)	C_a-C_b = 1.443 (5)
C(4)–C(3)	1.440 (6)	1.445 (5)	
C(6)–C(7)	1.446 (5)	1.437 (6)	
C(9)–C(8)	1.442 (6)	1.439 (6)	
C(11)–C(12)	1.434 (6)	1.442 (5)	
C(14)–C(13)	1.448 (5)	1.443 (5)	
C(16)–C(17)	1.447 (5)	1.440 (5)	
C(19)–C(18)	1.452 (5)	1.443 (5)	
C(2)–C(3)	1.359 (6)	1.359 (6)	C_b-C_b = 1.359 (5)
C(7)–C(8)	1.362 (6)	1.364 (6)	
C(12)–C(13)	1.363 (6)	1.352 (6)	
C(17)–C(18)	1.352 (6)	1.361 (6)	
C(4)–C(5)	1.390 (5)	1.379 (5)	C_a-C_m = 1.383 (6)
C(6)–C(5)	1.388 (5)	1.388 (5)	
C(9)–C(10)	1.389 (6)	1.386 (6)	
C(11)–C(10)	1.388 (6)	1.386 (5)	
C(14)–C(15)	1.379 (5)	1.368 (5)	
C(16)–C(15)	1.378 (5)	1.381 (5)	
C(19)–C(20)	1.391 (6)	1.381 (6)	
C(1)–C(20)	1.375 (6)	1.384 (6)	
C(2)–C(21)	1.502 (6)	1.512 (6)	$C_b-C_{\alpha,ethyl}$ = 1.501 (7)
C(3)–C(23)	1.510 (6)	1.494 (6)	
C(7)–C(25)	1.499 (6)	1.499 (6)	
C(8)–C(27)	1.506 (5)	1.489 (6)	
C(12)–C(29)	1.502 (6)	1.508 (5)	
C(13)–C(31)	1.495 (6)	1.499 (6)	
C(17)–C(33)	1.498 (6)	1.510 (6)	
C(18)–C(35)	1.496 (6)	1.496 (5)	
C(21)–C(22)	1.501 (7)	1.495 (7)	$C_{\alpha,ethyl}-C_{\beta,ethyl}$ = 1.513 (10)
C(23)–C(24)	1.486 (7)	1.512 (6)	
C(25)–C(26)	1.524 (6)	1.513 (6)	
C(27)–C(28)	1.515 (6)	1.519 (6)	
C(29)–C(30)	1.512 (6)	1.510 (6)	
C(31)–C(32)	1.528 (6)	1.517 (6)	
C(33)–C(34)	1.510 (6)	1.515 (6)	
C(35)–C(36)	1.512 (6)	1.516 (6)	

(25) See, for example: Ball, R. G.; Lee, K. M.; Marshall, A. G.; Trotter, J. *Inorg. Chem.* **1980**, *19*, 1463–1469.

(26) A compilation of terms used in describing porphyrin structural characteristics can be found in: Jameson, G. B.; Robinson, W. T.; Ibers, J. A. "Hemoglobin and Oxygen Binding"; Ho, C., Ed.; Elsevier: Amsterdam, 1982; pp 25–35.

(27) The twist angle is defined as the weighted mean of the N_x–Ru–Ru–N_x' (x = 1,4) torsion angles.

(28) Only the shortest interplanar atomic contact for each atom was considered in this tabulation.

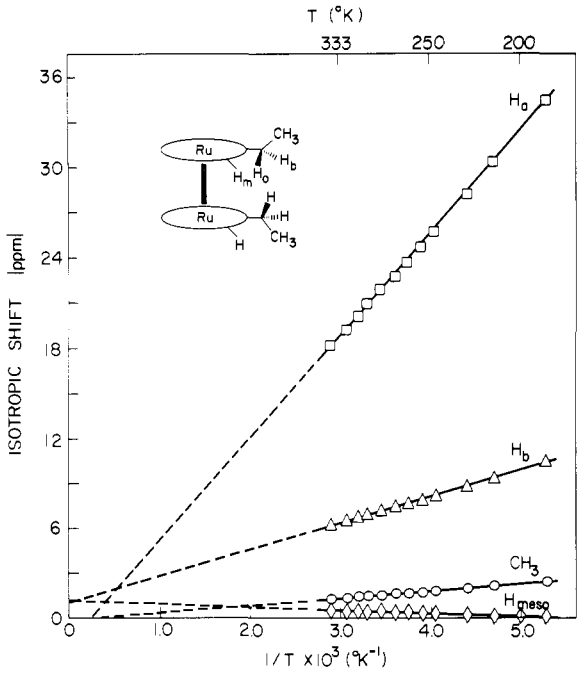

Figure 4. Isotropic shift vs. $1/T$ for $(Ru(OEP))_2$ in toluene-d_8.

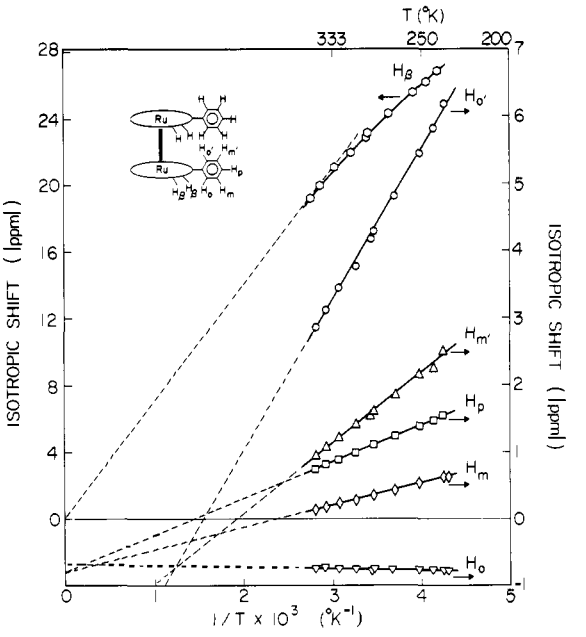

Figure 5. Isotropic shift vs. $1/T$ for $(Ru(TPP))_2$ in toluene-d_8.

Intramolecular bond distances (Table VII) and angles (Table VIII) are normal. The Ru–Ru′ bond length of 2.408 (1) Å is slightly longer than the 2.379 (1)-Å bond distance in $[Ru(C_{22}H_{22}N_4)]_2$,[30] the only other unbridged Ru(II) dimer reported to date.[31] The mean Ru–N distance (2.050 (5) Å) falls within the range of observed values for other ruthenium porphyrins (2.040 (6)–2.067 (14) Å).[3,5,8,32] The bond length pattern of the porphyrin macrocycles is typical for other metalloporphyrins.

Recently, there has been considerable interest in mapping experimental[33] and theoretical[34] deformation electron density in metal–metal bonded systems. Controversy has arisen because in some molecules that contain a metal–metal bond little or no significant charge accumulation between the metal atoms has been observed while in other systems charge density of appreciable magnitude has been mapped. Although the present data set is of relatively low resolution ($0.0 \leq \lambda^{-1} \sin\theta \leq 0.56$ Å^{-1}), it is interesting that in a final difference electron density summation[35] a significant charge accumulation (0.65 Å^{-3}) is observed between the metal atoms.

Discussion

The magnetic resonance and crystallographic results enable us to describe in detail the bonding in these binuclear ruthenium porphyrin dimers. We turn first to analysis of the ^{1}H NMR data, an analysis that is based on the extensive work of La Mar, Walker, Goff, and co-workers,[36–38] who have analyzed the NMR spectra of paramagnetic first-row metalloporphyrins.

Isotropic Shifts. Qualitatively, the large downfield shifts of the methylene protons in **5** and the large upfield shifts of the β-pyrrolic protons in **6** are indicative of large π-contact spin density at this position. The meso proton in **5** does not appear to be shifted. However, this can be caused by either negligible spin density at this position or mutually opposing and compensating shift contributions. Finally, although the meso phenyl proton shifts are relatively small, they are both upfield and downfield from the normal resonances.

Figures 4 and 5 illustrate the temperature dependencies of the isotropic shifts for $(Ru(OEP))_2$ and $(Ru(TPP))_2$. The strict linear behavior observed for all shifts except the β-pyrrolic protons indicates that the Curie law is obeyed by both complexes over the temperature range −90 to +95 °C. The small, low-temperature deviations from linearity exhibited by the β-pyrrolic proton shifts are similar to those observed for the intermediate-spin ferrous TPP complex[36] and are probably due to aggregation effects.[39] The rigorous adherence of all other shifts to the Curie law indicates that these dimers exist in a *single* spin state over the entire temperature range studied.

The small nonzero intercepts at $T^{-1} = 0$ exhibited by the OEP dimer **5** are all within the experimental error for these measurements. The extrapolated intercepts for meso phenyl positions, however, are significant. These deviations from the Curie law may reflect inherent differences between the diamagnetic rho-

(29) A referee brought to our attention the interesting case of the $(Cu(TPP\cdot)^+$ dimer (Scholz W. F.; Reed, C. A.; Lee, Y. J.; Scheidt, W. R.; Lang, G. *J. Am. Chem. Soc.* **1982**, *104*, 6791–6793). The separation between the mean planes of the two cores is 3.84 Å. In contrast to $(Ru(OEP))_2$, however, the two porphyrin macrocycles in the $(Cu(TPP\cdot))^+$ dimer are not coaxially arranged and a pronounced ruffling of porphyrin cores is observed. Although coupling of the porphyrin-centered unpaired spin with the d^9 system is observed in the solid state, the authors do not believe this to arise from intermolecular porphyrin π–π* interactions.

(30) Warren, L. F.; Goedken, V. L. *J. Chem. Soc., Chem. Commun.* **1978**, 909–910.

(31) (a) Cotton, F. A.; Walton, R. A. "Multiple Bonds between Metal Atoms"; Wiley: New York, 1982; pp 24, 197, 291. (b) Trogler, W. C. *J. Chem. Educ.* **1980**, *57*, 424–427.

(32) (a) Little, R. G.; Ibers, J. A. *J. Am. Chem. Soc.* **1973**, *95*, 8583. (b) Cullen, D.; Meyer, E. F.; Srivastava, T. S.; Tsutsui, M. *J. Chem. Soc., Chem. Commun.* **1972**, 584–585. (c) Ru(OEt)(TPP)(EtOH) and $[Ru(TPP)(OC_6H_4\text{-}p\text{-}CH_3)]_2O$, ref 4.

(33) For example: (a) Mitschler, A.; Rees, B.; Wiest, R.; Benard, M. *J. Am. Chem. Soc.* **1982**, *104*, 7501–7509. (b) Benard, M.; Coppens, P.; DeLucia, M. L.; Stevens, E. D. *Inorg. Chem.* **1980**, *19*, 1924–1930. (c) Troup, J. M.; Extine, M. W.; Ziolo, R. F. In "Electron Distributions and the Chemical Bond"; Coppens, P., Hall, M. B., Eds.; Plenum Press: New York, 1982. (d) Martin, M; Rees, B.; Mitschler, A. *Acta Crystallogr., Sect. B* **1982**, *B38*, 6–15. (e) Hino, K.; Saito, Y.; Benard, M. *Ibid.* **1981**, *B37*, 2164–2170.

(34) For example: Kok, R. A.; Hall, M. B. *Inorg. Chem.* **1983**, *22*, 728–734.

(35) Electron density maps were calculated with a locally modified version of NIELSAV (E. D. Stevens and W. K. Hansen), a program for the calculation of an exact three-dimensional Fourier summation in an oblique plane. In the calculation of the maps all unique intensities were used; those with negative values of F_o^2 were set to 0.

(36) (a) Goff, H.; La Mar, G. N.; Reed, C. A. *J. Am. Chem. Soc.* **1977**, *99*, 3641–3646. (b) Goff, H.; La Mar, G. N. *Ibid.* **1977**, *99*, 6599–6606.

(37) (a) La Mar, G. N.; Walker, F. A. *J. Am. Chem. Soc.* **1973**, *95*, 1782–1790. (b) La Mar, G. N.; Walker (Jensen), F. A. In "The Porphyrins"; Dolphin, D., Ed.; Academic Press: New York, 1979; Vol. IV, Part B, Chapter 2.

(38) (a) La Mar, G. N.; Eaton, G. R.; Holm, R. H.; Walker, F. A. *J. Am. Chem. Soc.* **1973**, *95*, 63–75. (b) La Mar, G. N.; Walker, F. A. *Ibid.* **1973**, *95*, 6950–6956. (c) Walker, F. A.; La Mar, G. N. *Ann. N.Y. Acad. Sci.* **1973**, *206*, 328–348. (d) Walker, F. A.; La Mar, G. N. *J. Am. Chem. Soc.* **1975**, *97*, 5103–5107.

(39) La Mar, G. N.; Visco, D. B. *J. Am. Chem. Soc.* **1974**, *96*, 7354–7355.

Table VIII. Selected Bond Angles (deg) for $(Ru(OEP))_2$

atoms	porphyrin 1	porphyrin 2	mean
N(1)-Ru-Ru	98.49 (8)	99.02 (9)	N-Ru-Ru = 98.4 (8)
N(2)-Ru-Ru	99.11 (9)	97.30 (9)	
N(3)-Ru-Ru	98.46 (9)	97.98 (8)	
N(4)-Ru-Ru	97.14 (9)	99.47 (9)	
N(1)-Ru-N(2)	88.5 (1)	88.7 (1)	N-Ru-N = 88.8 (2)
N(1)-Ru-N(4)	89.2 (1)	88.8 (1)	
N(2)-Ru-N(3)	88.8 (1)	88.9 (1)	
N(3)-Ru-N(4)	88.7 (1)	88.7 (1)	
N(1)-Ru-N(3)	163.1 (1)	163.0 (1)	163.3 (4)
N(2)-Ru-N(4)	163.8 (1)	163.2 (1)	
Ru-N(1)-C(1)	125.6 (3)	127.5 (3)	$Ru-N-C_a$ = 127.0 (5)
Ru-N(1)-C(4)	127.8 (3)	126.5 (3)	
Ru-N(2)-C(6)	126.7 (3)	126.8 (3)	
Ru-N(2)-C(9)	127.1 (3)	127.0 (3)	
Ru-N(3)-C(11)	127.2 (3)	127.6 (3)	
Ru-N(3)-C(14)	127.5 (3)	126.4 (3)	
Ru-N(4)-C(16)	126.7 (3)	127.0 (3)	
Ru-N(4)-C(19)	127.0 (3)	127.1 (3)	
N(1)-C(1)-C(2)	109.1 (3)	110.1 (4)	$N-C_a-C_b$ = 110.0 (3)
N(1)-C(4)-C(3)	110.4 (3)	109.9 (3)	
N(2)-C(6)-C(7)	110.0 (3)	110.2 (3)	
N(2)-C(9)-C(8)	110.2 (3)	109.9 (3)	
N(3)-C(11)-C(12)	110.6 (3)	110.1 (3)	
N(3)-C(14)-C(13)	110.3 (3)	109.6 (3)	
N(4)-C(16)-C(17)	109.8 (3)	110.2 (3)	
N(4)-C(19)-C(18)	109.9 (4)	110.0 (3)	
C(1)-N(1)-C(4)	106.5 (3)	106.1 (3)	C_a-N-C_a = 106.0 (4)
C(6)-N(2)-C(9)	106.2 (3)	106.1 (3)	
C(11)-N(3)-C(14)	105.3 (3)	106.0 (3)	
C(16)-N(4)-C(19)	106.2 (3)	105.8 (3)	
C(1)-C(2)-C(3)	107.1 (4)	107.1 (4)	$C_a-C_b-C_b$ = 107.0 (2)
C(4)-C(3)-C(2)	106.9 (4)	106.8 (4)	
C(6)-C(7)-C(8)	106.5 (4)	107.0 (4)	
C(9)-C(8)-C(7)	107.0 (3)	106.7 (4)	
C(11)-C(12)-C(13)	106.9 (4)	106.9 (3)	
C(14)-C(13)-C(12)	106.8 (4)	107.4 (4)	
C(16)-C(17)-C(18)	107.1 (4)	107.3 (3)	
C(19)-C(18)-C(17)	107.0 (3)	106.7 (3)	
N(1)-C(1)-C(20)	125.7 (4)	124.6 (4)	$N-C_a-C_m$ = 124.6 (5)
N(1)-C(4)-C(5)	124.7 (4)	125.0 (4)	
N(2)-C(6)-C(5)	125.4 (4)	124.7 (4)	
N(2)-C(9)-C(10)	124.8 (4)	124.5 (4)	
N(3)-C(11)-C(10)	124.0 (4)	124.1 (4)	
N(3)-C(14)-C(15)	124.2 (4)	124.9 (4)	
N(4)-C(16)-C(15)	124.5 (4)	124.2 (4)	
N(4)-C(19)-C(20)	124.3 (4)	124.6 (4)	
C(2)-C(1)-C(20)	125.1 (4)	125.3 (4)	$C_b-C_a-C_m$ = 125.3 (4)
C(3)-C(4)-C(5)	124.8 (4)	125.0 (4)	
C(7)-C(6)-C(5)	124.4 (4)	125.0 (4)	
C(8)-C(9)-C(10)	125.0 (4)	125.6 (4)	
C(12)-C(11)-C(10)	125.3 (4)	125.8 (4)	
C(13)-C(14)-C(15)	125.5 (4)	125.3 (4)	
C(15)-C(16)-C(17)	125.6 (4)	125.5 (4)	
C(18)-C(19)-C(20)	125.8 (4)	125.3 (4)	
C(1)-C(20)-C(19)	126.9 (4)	127.0 (4)	$C_a-C_m-C_a$ = 127.0 (4)
C(4)-C(5)-C(6)	126.2 (4)	126.7 (4)	
C(9)-C(10)-C(11)	127.1 (4)	127.4 (4)	
C(14)-C(15)-C(16)	127.4 (4)	127.3 (4)	
C(1)-C(2)-C(21)	125.2 (4)	125.5 (4)	$C_a-C_b-C_{\alpha,ethyl}$ = 125.5 (12)
C(4)-C(3)-C(23)	126.3 (4)	124.9 (4)	
C(6)-C(7)-C(25)	125.2 (4)	125.2 (4)	
C(7)-C(8)-C(27)	127.4 (4)	128.5 (4)	
C(11)-C(12)-C(29)	125.4 (4)	125.3 (4)	
C(14)-C(13)-C(31)	125.3 (4)	124.2 (4)	
C(16)-C(17)-C(33)	125.0 (4)	125.0 (4)	
C(19)-C(18)-C(35)	125.3 (4)	124.8 (4)	

Table VIII (*Continued*)

atoms	porphyrin 1	porphyrin 2	mean
C(3)-C(2)-C(21)	127.6 (4)	127.4 (4)	C_b-C_b-$C_{\alpha,ethyl}$ = 127.8 (5)
C(2)-C(3)-C(23)	126.6 (4)	128.2 (4)	
C(8)-C(7)-C(25)	128.3 (4)	127.8 (4)	
C(7)-C(8)-C(27)	127.4 (4)	128.5 (4)	
C(13)-C(12)-C(29)	127.7 (4)	127.7 (4)	
C(12)-C(13)-C(31)	127.7 (4)	128.3 (4)	
C(18)-C(17)-C(33)	127.9 (4)	127.5 (4)	
C(17)-C(18)-C(35)	127.7 (4)	128.4 (4)	
C(2)-C(21)-C(22)	113.0 (4)	112.8 (4)	C_b-$C_{\alpha,ethyl}$-$C_{\beta,ethyl}$ = 113.6 (10)
C(3)-C(23)-C(24)	114.2 (4)	114.4 (4)	
C(7)-C(25)-C(26)	114.0 (4)	112.8 (4)	
C(8)-C(27)-C(28)	115.4 (3)	113.9 (4)	
C(12)-C(29)-C(30)	113.2 (4)	112.9 (4)	
C(13)-C(31)-C(32)	111.3 (4)	113.2 (4)	
C(17)-C(33)-C(34)	114.6 (4)	112.9 (4)	
C(18)-C(35)-C(36)	114.4 (4)	112.9 (4)	

dium(II) dimers[17] used to reference the isotropic shifts and small temperature-independent shift contributions from second-order Zeeman interactions or both.[40]

Dipolar Shifts. In the limit of axial symmetry, the dipolar shift is given by[41]

$$\left(\frac{\Delta H}{H}\right)_{\text{dipolar}} = -\frac{1}{3N}(\chi_{\parallel} - \chi_{\perp})\frac{3\cos^2\theta - 1}{r^3} \qquad (1)$$

where $\chi_{\parallel}$ and $\chi_{\perp}$ are the principal susceptibilities parallel and perpendicular to the unique axis, r is the length of the metal-proton vector, and θ is the the angle between this vector and the principal axis of the molecule. La Mar and Walker[37a] observed that meso phenyl rings of paramagnetic TPP complexes are effectively insulated from π-contact spin density in the porphyrin ring. Using this observation they were able to develop a geometric model for the dipolar shift whereby the measurment of the pure dipolar shift for a single meso phenyl proton and evaluation of its geometric factor quantitatively determine the dipolar shift for any other position on the porphyrin and provide a measure of the magnetic anisotropy for the complex. This model, with the origin located at the metal center, is not applicable to the present situation, where two porphyrin macrocycles are held together in a cofacial, coaxial manner. No model having a single origin located at either metal center can account for the small upfield shift observed for the H_o resonance and the large downfield shift of the $H_{o'}$ (Table VI). Therefore, it was necessary to develop a new geometric model.

The critical features of the phenyl shifts in $(Ru(TPP))_2$ and $(Ru(TTP))_2$ that must be accounted for by a dipolar shift model are the unequal and oppositely directed shifts for the H_o and $H_{o'}$ protons and the relative magnitudes of all phenyl proton shifts. The model for monomeric metalloporphyrins fails because it does not account for the loss of mirror symmetry in the porphyrin plane. Two geometric models that do account for loss of mirror symmetry are (i) a two-center model having each origin located on the axial symmetry axis and equidistant from the pseudo center of symmetry (the midpoint of the Ru–Ru bond) and (ii) a single-center model where the origin is placed directly at this pseudo center of symmetry (Figure 6). Both of these models require accurate values for the angular and radial parameters defined in eq 1 and illustrated in Figure 6. The physical dimensions of the porphyrin macrocycle in many different metal complexes have been determined by X-ray methods.[42] The overall structure of the macrocycle does not deviate dramatically among the various complexes. Therefore the critical information required in Figure 6 is the distance between the two macrocycles in the present dimers. An estimate of this distance for the TPP analogue **6** can be obtained from the X-ray structure of $(Ru(OEP))_2$. The mean interplanar spacing should be the sum of the Ru–Ru bond distance plus the displacements of the Ru atoms from the calculated least-squares planes: 2.41 + 0.42 + 0.43 = 3.26 Å. With this distance the geometric factors for both models illustrated in Figure 6 were calculated.[43]

As indicated in Figure 6A the first model was tested with the two origins placed at the metal centers. We observed that this model did not adequately describe the shifts of the H_o and $H_{o'}$ protons. The contribution of the origin closest to these two protons dominates the final geometric factor. This results in calculated geometric factors similar to those of the monomeric metalloporphyrin model, i.e., geometric factors that are similar in magnitude and in the same direction.

The second model possesses a single origin placed midway between the two Ru atoms (Figure 6B). The geometric factors calculated according to this model are summarized in Table IX. This model successfully predicts unequal dipolar shifts in opposite directions for the *o*- and *o'*-phenyl positions, in agreement with the observed shifts. A plot of the geometric factors vs. isotropic shifts for the phenyl protons reveals an excellent correlation for every position except the $H_{o'}$ shift (Figure 7). The calculated geometric factor predicts a larger dipolar shift than is actually observed for the *o'*-phenyl position. The shift for this position, however, may be very sensitive to steric and electronic differences between the diamagnetic reference complexes and these dimers and possibly to inaccuracies in the approximations required to obtain the geometric parameters. There may also be small leakage of contact spin density from the meso carbon atom into the meso phenyl ring. From the approximate correlation of shift and geometric factor we assign this resonance to the ortho′ phenyl proton that points into the region between the two porphyrin planes nearest the two ruthenium atoms. Because of the excellent correlation of all other phenyl shifts, we believe that these shifts are predominantly dipolar in origin. When we assume that the electronic structures and magnetic anisotropies are similar for dimers **5** and **6**, then the dipolar shift contribution to any position in these dimers may be calculated according to the model illustrated in Figure 6B and eq 1. Subtraction of the dipolar shift from the isotropic shift yields the value of the contact shift for each position, as listed in Table X.

Magnetic Anisotropy. The sign of the dipolar shift is observed to follow that of the geometric factor for every position in **5** and **6**. Equation 1, which is based on the assumption of axial symmetry, predicts that $\chi_{\perp} > \chi_{\parallel}$. If the anisotropy of the magnetic susceptibility between these dimers does not differ significantly, it may be calculated directly from the *m'*-phenyl shift (1.53 ppm) and geometric factor (-2.32×10^{-21} cm^{-3}). From eq 1 we have $\chi_{\parallel} - \chi_{\perp} = -1120 \times 10^{-6}$ cgs units. The average magnetic moment

(40) Horrocks W. D. Jr.; Greenberg, E. S. *Biochim. Biophys. Acta* **1973**, *322*, 38–44.

(41) Jesson, J. P. In ref. 19, Chapter 1.

(42) (a) Fleischer, E. B. *Acc. Chem. Res.* **1970**, *3*, 105–112. (b) Hoard, J. L. *Science (Washington, D.C.)* **1971**, *174*, 1295–1302.

(43) An additional calculation of r and θ was performed from the domed porphyrin macrocyclic structure observed for **5** in the solid state with perpendicular phenyl rings placed in the meso positions. The results were virtually identical with those from the simpler model described in the text.

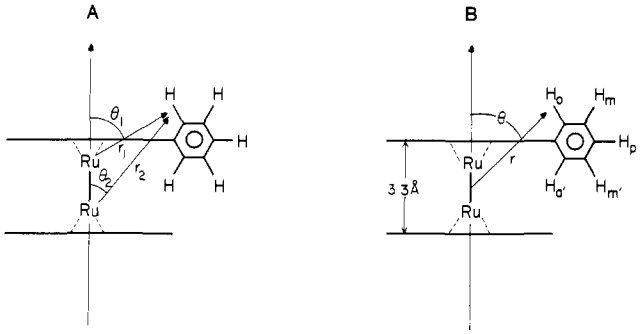

Figure 6. Dipolar reference models for $(Ru(TPP))_2$.

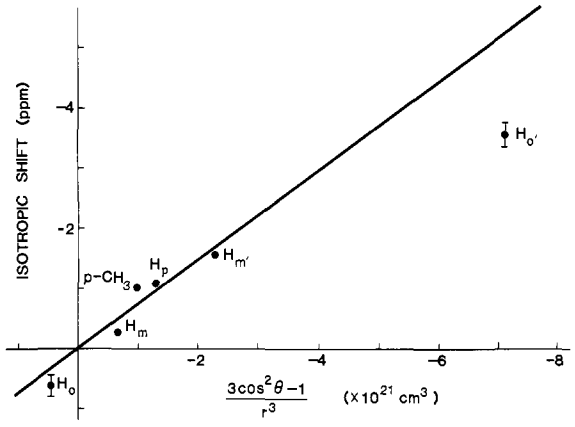

Figure 7. Plot of isotropic shifts for *meso*-aryl substituents in $(Ru(P))_2$ vs. calculated geometric factors according to Figure 6B.

Table IX. Calculated Geometric Factors from Model Illustrated in Figure 6B

	position	r,[a] Å	θ, deg	$(3\cos^2\theta-1)/r^3$ ($\times 10^{21}$ cm^3)
TPP	o	6.33	53.59	+0.22
	m	8.39	64.85	−0.77
	p	8.94	79.50	−1.26
	m′	7.52	93.76	−2.32
	o′	5.12	95.87	−7.21
TTP	p-CH_3	9.73	80.36	−0.99
OEP	H_{meso}	4.80	70.14	−5.93
TPP	H_β	5.52	72.82	−4.40
CH_2CH_3 of OEP	αCH_2	⟨6.51⟩[b]	⟨75.41⟩[b]	⟨−2.93⟩
	αCH_3	⟨7.42⟩[b]	⟨77.4⟩[b]	⟨−2.01⟩

[a] Calculated from the data in ref 37a. See also ref 42. [b] Averaged values assuming free rotation.

$\bar{\mu}_{corr}$ for $(Ru(OEP))_2$ in benzene solution has been reported as 2.8 μ_B.[4] From this value the average susceptibility, $^1/_3(\chi_\parallel + 2\chi_\perp)$, is 3268×10^{-6} cgs units. We thus obtain $\chi_\parallel = 2520 \times 10^{-6}$ cgs units and $\chi_\perp = 3640 \times 10^{-6}$ cgs units, where the uncertainty is estimated to be approximately ±15%. If we assume that the contribution to the anisotropy from second-order Zeeman interactions is small,[36a] then we may calculate the magnetic moments and effective g values ($S = 1$) associated with $\chi_\parallel$ and $\chi_\perp$ to be $\mu_\parallel = 2.46\ \mu_B$ ($g_\parallel = 1.71$) and $\mu_\perp = 2.95\ \mu_B$ ($g_\perp = 2.1$).

These estimates of the g values for the triplet spin system in $(Ru(OEP))_2$ are within the range of normal X-band EPR spectrometers. No signals were observed, however, for frozen toluene solutions of $(Ru(OEP))_2$ at ~10 K. Fast electron relaxation from zero-field-splitting modulation may broaden these signals beyond observability, even at 10 K. A more detailed analysis of the magnetic anisotropy exhibited by these complexes must await temperature-dependence studies of the magnetic susceptibilities of **5** and **6**.

Spin Transfer and Ru–P π Bonding. The shift patterns observed in metalloporphyrins for various unpaired electron configurations of first-row metals are well-known. The information pertaining to these systems can be summarized as follows. The presence of unpaired electrons in the $3d_{x^2-y^2}$ orbital always results in large σ-contact shifts around the porphyrin ring. Examples are found in high-spin Fe(II), $S = 2$ and Fe(III), $S = {}^5/_2$ porphyrins. Unpaired electrons in either the $3d_{xz}$ or $3d_{yz}$ orbitals result in π-contact shifts, as observed for high-spin Mn(III), $S = 2$, low-spin Fe(III), $S = {}^1/_2$, and intermediate-spin Fe(II), $S = 1$ porphyrins. Finally the presence of unpaired electrons in either the $3d_{z^2}$ or $3d_{xy}$ orbitals produces only small contact shifts that are in most cases completely overshadowed by either of the two other shift mechanisms. The origin of π-contact shifts in metalloporphyrins can be further delineated. Spin transfer derived from P $3e(\pi) \rightarrow$ M charge transfer leads to large spin density in the pyrrole rings and a node at the meso carbon atoms.[37b] Spin transfer derived from M → P $4e(\pi^*)$ charge transfer (classic back-bonding) leads to large π-spin density at the meso carbon atoms and less in the pyrrole ring.

Table X. Contact and Dipolar Contributions to Observed Shifts[a]

position	$\lvert\Delta H/H\rvert$ obsd	$\lvert\Delta H/H\rvert$ dipolar[b]	$\lvert\Delta H/H\rvert$ contact	$\lvert A\rvert/h \times 10^{-5}$ Hz
meso o	0.6	0.44	~0.0	
m	0.3	0.40	~0.0	
p	1.1	0.92	~0.0	
m′	1.5	1.79	~0.0	
o′	3.60	5.84	2.2	
p-CH_3	1.04	0.72	~0.0	
H_{meso}	0.9	3.64	2.74	0.39
H_β	22.8	2.90	25.7	3.6
β-CH_2CH_3	21.3	2.02	19.28	7.1
	7.0	2.02	5.0	2.7
β-CH_2CH_3	1.5	1.46	~0.0	

[a] Shifts in ppm, in benzene-d_6 or toluene-d_8 at 25 °C; downfield shifts are positive. [b] All phenyl proton shifts were assumed to be purely dipolar except for the o′ position. Calculation of dipolar shift for this and other positions is based on the best least-squares fit to the data plotted in Figure 7.

Although these correlations are clearly established for first-row metalloporphyrins, to our knowledge no similar NMR analyses of paramagnetic metalloporphyrins have been reported for second- or third-row metals. We find that these correlations do indeed carry over very well to the metal d-orbital systems present in **5** and **6**, and we use this information in support of a simple description of the metal–metal interactions in **5** and **6**. The calculated contact shifts and associated hyperfine coupling constants for **5** and **6** are listed in the last two columns of Table X. The roughly equal, but opposite, shifts observed for β-pyrrolic substituents provide strong evidence for large positive π spin density in the pyrrole rings. The small positive contact shift calculated for the meso position indicates the presence of small positive contact spin density. There is no evidence for σ spin density at any position in the proton shifts of these complexes. It is interesting to note that whereas intermediate-spin Fe(II),[36] $S = 1$ and high-spin Mn(III),[38] $S = 2$ porphyrins exhibit π-contact shifts in the pyrrole rings that are very similar to those observed in **5** and **6**, they also exhibit large downfield shifts for the meso protons. These downfield shifts have been ascribed to correlation effects. With the data at hand we are unable to explain the absence of such correlation effects in **5**. Attempts to obtain the NMR spectrum of $(Ru(T\text{-}n\text{-}PrP))_2$ to probe further the nature of unpaired spin density at this position have been frustrated by solubility problems. The magnitude of spin density at the meso position in **5** appears to be relatively small, however, and will not be discussed further. The exclusive π spin transfer observed for **5** and **6** requires that unpaired spin reside in the "molecular" orbitals derived from a Ru_2^{4+} unit that also has π symmetry. We believe that these molecular orbitals are expected to be derived from the Ru $4d_{xz}$ and $4d_{yz}$ AO's that are engaged in the formation of a metal–metal bond.

Molecular Orbital Scheme. It is useful to review the evidence from above as it pertains to the bonding in these binuclear ruthenium porphyrin dimers. The crystal structure of **5** and chemical titration data[4] indicate that the ruthenium oxidation state in

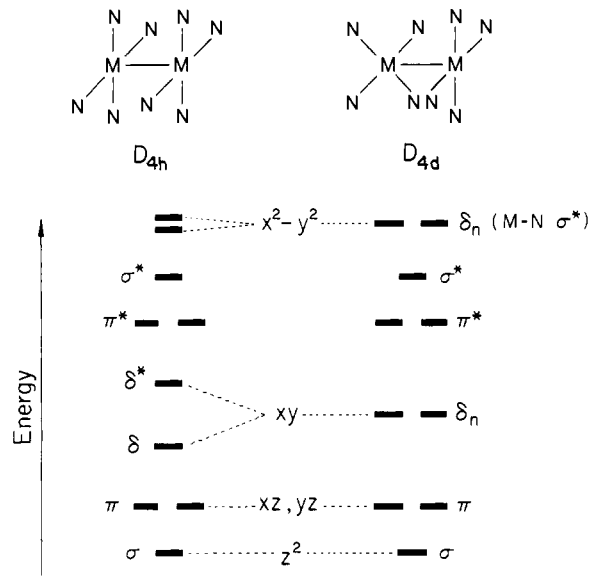

Figure 8. Molecular orbital diagram for the ruthenium orbitals in $(Ru(P))_2$ (d^{12}).

$(Ru(OEP))_2$ is +2, corresponding to a 12-electron system for the Ru_2^{4+} core. The 2.408 (1)-Å distance separating the two Ru atoms indicates a strong metal–metal bond exists that holds the halves of the dimer together.[44] The bonding deformation maps, which show π symmetry, suggest considerable charge buildup between the Ru atoms. The Curie behavior of **5** and **6** and the symmetry of the contact shifts require that the paramagnetism of these complexes originate from a single spin state with π symmetry. The measured value of the average magnetic moment is 2.8 μ_B. The most reasonable spin state for these even-electron systems that is in line with the susceptibility data is an $S = 1$ triplet system.

A molecular orbital scheme that accounts for all of the above data is one in which a multiple metal–metal bond is present between the two Ru atoms. A well-known, qualitative scheme for multiple bonding between metal atoms is shown in Figure 8.[31b,44] The top of Figure 8 schematically illustrates fully eclipsed and staggered conformational orientations of ligands around the binuclear core. Here N represents the pyrrolic nitrogen atoms of the porphyrin ring. For clarity the other atoms of the macrocycles are not shown. If all N–M and M–M distances remain unchanged, then rotation around the M–M bond causes only the relative energies of the δ and δ^* orbitals to change. It has been shown[45] that an eclipsed conformation is required for maximum δ bonding and that the δ and δ^* orbitals smoothly converge to form a pair of degenerate nonbonding orbitals in the fully staggered conformation. The $4d_{z^2}$-derived M–M σ bond and $4d_{xz}$,d_{yz}-derived π bonds are not affected by rotation about the M–M bond because they possess effective cylindrical symmetry around the bond axis. The relative splitting of σ,σ^*, π,π^*, and δ,δ^* orbital pairs reflects the normally observed dominance of σ bonding followed by π bonding in similar binuclear systems containing multiple M–M bonds.[45] An assumption inherent in this MO scheme is that metal–metal interactions are the dominant factors in determining relative orbital energies. The porphyrin ligand, therefore, provides an effective square-planar coordination geometry around each metal atom in this simple model[46] (see below). Since the ruthenium(II) systems of **5** and **6** contribute 12 electrons to the different energy levels, the degenerate $e_g(\pi^*)$ MO's are left half-filled in either conformation. A spin triplet ground state ($^3A_{2g}$) with π symmetry is predicted, in accordance with the experimental data. The crystal structure of **5** shows that the two porphyrin planes are neither completely staggered nor eclipsed but are twisted 23.8 (1)°.[27] Thus if the peripheral ethyl groups are neglected, the effective symmetry environment around the metal core is reduced to D_4 and the actual MO diagram for **5** should lie between the two shown in Figure 8. In this scheme no information concerning metal–metal bonding is obtainable from the twist angle because the δ and δ^* components are both filled. Moreover there is neither a preference for any specific conformation nor a barrier to rotation around this bond because of metal–metal bonding. Between the two Ru atoms a formal double bond ($a_{1g}^2e_u^4b_{1g}^2b_{1u}^{*2}e_g^{*2}$) composed of three bonding components ($\sigma + 2\pi$) and one antibonding component (π^*) is predicted to exist.

In this scheme the degenerate π^* orbitals that contain the unpaired spins exhibit a nodal plane that bisects the Ru–Ru bond and is oriented perpendicular to it. The dipolar geometric model (Figure 6B) that successfully models the phenyl shifts has its origin at the point where this plane intersects the Ru–Ru bond. Since there should be no net unpaired spin density at this point, the question arises as to how this model accounts for these shifts. The dipolar interactions between an electron and proton is purely a "through space" interaction.[41] Therefore, the origin of the model need not lie on an atom or be directly related to the bonding system between the unpaired electrons and proton. The choice of origin must, however, be consistent with the symmetry of the molecule. This restriction leaves only the pseudo center of symmetry and the points situated symmetrically around this point on the C_4 axis as suitable choices. This model, then, must effectively average the dipolar contributions from the two regions of unpaired spin density surrounding the origin to a particular position of the complex.

The dominant P $3e(\pi) \rightarrow$ M π charge transfer responsible for spin transfer in the contact shifts for **5** and **6** places the P $3e(\pi)$ MO slightly above the π^* metal MO's. Note that osmium(II) porphyrin dimers,[17] analogous to the Ru dimers described here show dominant Os $\pi \rightarrow$ P $4e(\pi^*)$ back-bonding interactions.[38] The absence of any σ contact shifts in **5** or **6** indicates that the MO's derived from the Ru $d_{x^2-y^2}$ AO's are unoccupied. From theoretical calculations for similar systems[47a,48] we have tentatively placed these MO's above the σ^* component of the metal–metal bond in Figure 8. A more detailed discussion of the relative energies of these unoccupied levels awaits further spectroscopic and theoretical studies.

The results of two recent theoretical studies are relevant to the properties of the binuclear porphyrin dimers described here. The first is an extended-Hückel calculation for bridged porphyrin dimers by Tatsumi and Hoffmann.[48] Although their calculations were for iron porphyrin systems, at one stage of their analysis they considered the interaction of two four-coordinate iron porphyrin monomers in direct analogy to **5**. The MO diagram they presented for this arrangement is very similar to the one presented in Figure 8. The Fe–Fe distance used in their study was ~3.3 Å, which is considerably longer than the Ru–Ru distance observed in **5** (2.41 Å). This difference should cause all the calculated orbital splittings to be smaller than are present in the complexes described here. Nevertheless, the same triplet ground state with π symmetry is predicted for the analogous $(Fe(P))_2$ dimer, indicating that the types of M–M bonding interactions for these systems should be similar. Yet four-coordinate ferrous porphyrins show no tendency to dimerize, either in the solid state[49] or in solution at room temperature.[38b] In fact, no well-characterized divalent, four-coordinate metalloporphyrins involving first-row metals are known to dimerize and form metal–metal bonds at room temperature.[50]

(44) Reference 31a, Chapter 8.
(45) Cotton, F. A. *Chem. Soc. Rev.* **1975**, *4*, 27–53.
(46) The solid-state structure of $Ru(OEP))_2$ shows the ruthenium atoms to be significantly displaced from the center of the mean plane of the porphyrin macrocycles in contrast to the model described here. The effect of this difference will be manifested mainly in the energy of the $d_{x^2-y^2}$ orbital. Theoretical calculations (ref 50) indicate that moving the metal away from the porphyrin core stabilizes the $d_{x^2-y^2}$ orbital but does not affect the energies of the d_{xz}, d_{yz}, d_{xy}, and d_{z^2} orbitals significantly. Since the $4d_{x^2-y^2}$ derived MO's are not occupied in the present case the conclusions reached here about the ground state of the porphyrin dimers should not be affected by this difference.

(47) (a) Norman J. G., Jr.; Renzoni, G. E.; Case, D. A. *J. Am. Chem. Soc.* **1979**, *101*, 5256–5267. (b) Cotton, F. A.; Pedersen, E. *Inorg. Chem.* **1975**, *14*, 388–391.
(48) Tatsumi, K.; Hoffmann, R. *J. Am. Chem. Soc.* **1981**, *103*, 3328–3341.
(49) Collman, J. P.; Hoard, J. L.; Kim, N.; Lang, G.; Reed, C. A. *J. Am. Chem. Soc.* **1975**, *97*, 2676–2681. Kirner, J. F.; Reed, C. A.; Scheidt, W. R. *Ibid.* **1977**, *99*, 1093–1101.

The contrast in the tendency of second- and third[18]-row metalloporphyrins to form metal–metal bonds as opposed to first-row analogues under the same conditions may be rationalized by the overlap requirements[31b,44] of metal–metal bond formation and the relative sizes of the 3d vs. 4d and 5d AO's. However, an investigation of four-coordinate first-row metalloporphyrins at *low temperature* to determine whether they too might form metal–metal bonds is warranted.

The second theoretical study of interest here concerns the electronic structures of $Ru_2(O_2CR)_4^+$ and $Rh_2(O_2CR)_4^+$ complexes.[47a] These complexes are classic examples of binuclear carboxylates $M_2(O_2CR)_4L_2$ that contain multiple metal–metal bonds. The Ru_2^{3+} unit in the carboxylate complex represents the mixed-valent couple Ru^{II}/Ru^{III} and thus is the once-oxidized equivalent of the Ru_2^{4+} unit in $(Ru(P))_2$. The bridging carboxylate ligands enforce an eclipsed conformation in $Ru_2(O_2CR)_4^+$, in contrast to the twisted conformation observed for **5** in the solid state. This structural difference manifests itself in the electronic structure of the $Ru_2(O_2CR)_4^+$ by increasing the energy splitting between the δ and δ^* components of the metal–metal bond.

A SCF–Xα–SW calculation[47a] accounts for the quartet ground state of $Ru_2(O_2C_2H_3)_4^+$ [47b] in that it predicts that the δ^* orbital is slightly higher than the π^* orbital and that the degenerate M–M π^* orbitals and δ^* orbital are singly occupied. The destabilization of the δ^* orbital relative to the π^* d-orbital combination arises from significant interactions of the δ^* orbital with several carboxylate orbitals. Thus, in $Ru_2(O_2CR)_4^+$ complexes Norman et al.[47a] conclude that the normal $\delta^* < \pi^*$ ordering, which is predicted by metal–metal bonding considerations alone, is significantly perturbed by interactions with the carboxylate ligands. In the present complexes, however, the porphyrin MO's do not appear to interact in the same way or as strongly as do the carboxylate ligand with the Ru_2^{n+} unit. Further theoretical calculations on $(Ru(P))_2$ species are of obvious interest.

Summary and Conclusions

A convenient synthesis of several new paramagnetic ruthenium porphyrin dimers is described and an analysis of their proton NMR spectra is presented. The complementary nature of the substituent patterns and paramagnetic shifts observed for $(Ru(OEP))_2$ and $(Ru(TPP))_2$ allows the isotropic shift to be broken down into its contact and pseudocontact constituents. The dipolar shifts have been calculated for these dimers and their magnetic anisotropies have been estimated. From our analysis of the contact shifts we have developed a qualitative MO diagram for the metal–metal bonding between the two ruthenium atoms in these dimers that both accounts for their magnetic properties and indicates that the formal Ru–Ru bond order is 2. The crystal structure of $(Ru(OEP))_2$ verifies the overall dimeric structural model indicated by the NMR analysis and supports the simple model for metal–metal bonding. Also, experimental X-ray deformation density maps, calculated in the vicinity of the metal atoms, have features that can be interpreted in terms of strong charge density accumulation between the ruthenium atoms.

These results suggest several interesting areas for future study. The metal–metal bonding scheme in Figure 8 is compatible with a wide range of d-electron counts. Thus other combinations of second- and third-row metals may produce stable dimers. The properties of the porphyrin macrocycle and absence of bridging ligands produce an environment around the M–M bond that is well suited for the study of both bond strengths and dynamics. Investigations into these areas as well as into the reactivity of these dimers are in progress.

Acknowledgment. We are grateful to the National Institutes of Health, Grant CH-17880 (J.P.C.) and Grant HL-13157 (J. A.I.), for support of this research.

Registry No. 1, 89530-39-2; **2**, 89555-37-3; **3**, 54762-60-6; **4**, 34690-41-0; **5**, 54762-43-5; **5**·$2C_5H_{12}$, 89530-40-5; **6**, 80004-21-3; $(Ru(TTP))_2$, 80004-22-4; Ru, 7440-18-8.

Supplementary Material Available: Positional parameters for the non-hydrogen atoms (Table II), anisotropic thermal parameters (Table III), hydrogen atom parameters (Table IV), the final values of $10|F_o|$ and $10|F_c|$ (Table V), and a stereoscopic packing diagram (Figure 2) (43 pages). Ordering information is given on any current masthead page.

(50) Reed, C. A.; Kouba, J. K.; Grimes, C. J.; Cheung, S. K. *Inorg. Chem.* **1978**, *17*, 2666–2670.